Analysis of Power-Maximizing Region 2 Controllers for Wind and Marine Turbines

Journal of Physics: Conference Series **2767** (2024) 032051 doi:10.1088/1742-6596/2767/3/032051

Analysis of Power-Maximizing Region 2 Controllers for Wind and Marine Turbines

David Stockhouse[1,2*], Daniel Zalkind[2], Hannah Ross[2], and Lucy Pao[1]

[1]University of Colorado Boulder, Boulder, CO, USA
[2]National Renewable Energy Laboratory, Golden, CO, USA

E-mail: *David.Stockhouse@colorado.edu

Abstract. Wind and marine energy are rapidly growing and complementary technologies that share some techniques for simplified modeling and control, particularly in below-rated flow speeds. A turbine operator has several choices of controller for maximizing power in Region 2. The simple and ubiquitous $K\Omega^2$ control law is often effective but limited in its flexibility. Alternative controllers use reference tracking to split the control objectives into a low-bandwidth optimal tip-speed ratio tracking loop to maximize steady-state power and a higher-bandwidth proportional-integral control loop to reject inflow turbulence. Several options exist for identifying the slowly varying optimal set point during operation, based on estimating the inflow velocity or filtering the power or torque signals. This study compares the trade-offs between performance and other design priorities for a few choices of reference-tracking controller in the literature for reference wind and marine turbines. Analysis is performed in the frequency domain using the linearization of each controller, and the impact of turbulent disturbances on the closed-loop system is described. The controllers are simulated in OpenFAST to analyze their performance with higher-order nonlinear turbine dynamics.

1. Introduction

Several countries around the world are seeking to grow their renewable energy production in the near future, with relatively mature wind energy at the forefront of much development. Marine turbines are a promising and similar but lesser-established technology that capture energy from flowing water instead of wind. The United States has enough marine power potential to supply more than 50% of the country's current energy needs [1], but little development has been performed so far. The field is progressing by adapting many principles of design and operation from wind energy that have been de-risked and proven to efficiently capture power.

The most common technology for both wind and marine energy capture is the axial-flow turbine, where the direction of fluid flow is aligned with the axis of rotation of the rotor (a horizontal-axis wind turbine in wind energy). The principle of operation is the same for wind and marine axial-flow turbines, so the analysis made in this work is intentionally generic to be applied to either. Although there are several practical differences between operating wind and marine turbines, the same control schemes can be used for maximizing below-rated power. The Reference Open-Source Controller (ROSCO) [2] is a widely used wind turbine controller (recently adapted to marine turbines with modification of the simulation tool OpenFAST [3]) that has multiple torque controller configurations in Region 2. The ROSCO toolbox features autotuning to facilitate convenient control design, but the controller configuration is chosen

manually. The purpose of this work is to analyze several torque controller configurations to investigate their trade-offs in controlling wind and marine turbines.

In Section 2, the simplified axial-flow turbine model is presented along with a number of controllers for driving the rotor speed to the optimal set point. In Section 3, the dynamics of the system and controllers are linearized around the power-maximizing operating points, and the closed-loop components of the system are investigated in the frequency domain. In Section 4, the controllers are simulated using the mid-fidelity modeling tool OpenFAST [3], and the conclusions and future work are discussed in Section 5.

2. Background

The power extracted by an axial-flow turbine depends on the power coefficient C_p, a nonlinear function of the tip-speed ratio (TSR) λ and blade pitch β. In Region 2, the C_p-function is maximized at a particular TSR λ^* and blade pitch β_{fine}, so the controller maximizes power by keeping blade pitch constant at $\beta = \beta_{\text{fine}}$ and regulating the rotor speed to maintain $\lambda \approx \lambda^*$. With β fixed, C_p is only a function of TSR, related to the flow speed v and rotor speed Ω by $\lambda = \frac{R\Omega}{v}$, where R is the rotor radius (blade length), so the optimal rotor-speed set point is $\Omega^* = \frac{\lambda^* v}{R}$. The power flowing into the rotor is

$$P_{\text{rot}}(\Omega, v) = \frac{1}{2}\rho\pi R^2 v^3 C_p(\Omega, v), \tag{1}$$

where ρ is the fluid density. This induces the rotor inflow torque $T_{\text{rot}}(\Omega, v) = \frac{P_{\text{rot}}(\Omega,v)}{\Omega}$ resisted by the controllable generator torque τ through a geared drivetrain. The drivetrain may also include a gearbox to step up the rotor speed into the generator by the ratio N_{gb}, making the generator speed $N_{\text{gb}}\Omega$. The generator power flowing out of the system is

$$P(\Omega, \tau) = N_{\text{gb}}\Omega\tau, \tag{2}$$

and torque balance causes the dynamics

$$J_{\text{rot}}\dot{\Omega} = T_{\text{rot}}(\Omega, v) - N_{\text{gb}}\tau, \tag{3}$$

where J_{rot} is the rotational inertia of the rotor-generator system.

2.1. Region 2 Operating Schedule

In order to maximize power in Region 2, the steady-state operating schedule for the controller should follow the peak of the C_p-function. Under fixed blade pitch, the C_p-function has a maximum C_p^* at a particular TSR λ^* that is usually constant throughout Region 2. Respecting the steady-state-optimal TSR generates a unique monotonically increasing relationship between the flow speed $\overline{v}$, rotor speed $\overline{\Omega}$, generator torque $\overline{\tau}$, and generator power $\overline{P}$, resulting in

$$\overline{\Omega} = \Omega^* = \frac{\lambda^* \overline{v}}{R}, \tag{4}$$

$$\overline{P} = \frac{1}{2}\frac{\rho\pi R^5 C_p^*}{(N_{\text{gb}}\lambda^*)^3}\left(N_{\text{gb}}\overline{\Omega}\right)^3 := K\left(N_{\text{gb}}\overline{\Omega}\right)^3, \tag{5}$$

$$\overline{\tau} = K\left(N_{\text{gb}}\overline{\Omega}\right)^2. \tag{6}$$

These steady-state monotonic relationships in Eqs. (4)–(6) are used in the following sections to define the operating point schedule used by the Region 2 controller. Fig. 1 illustrates these steady-state relationships in the context of rotor performance for the Technical University of Denmark (DTU) 10 MW and Reference Model 1 (RM1) turbines.

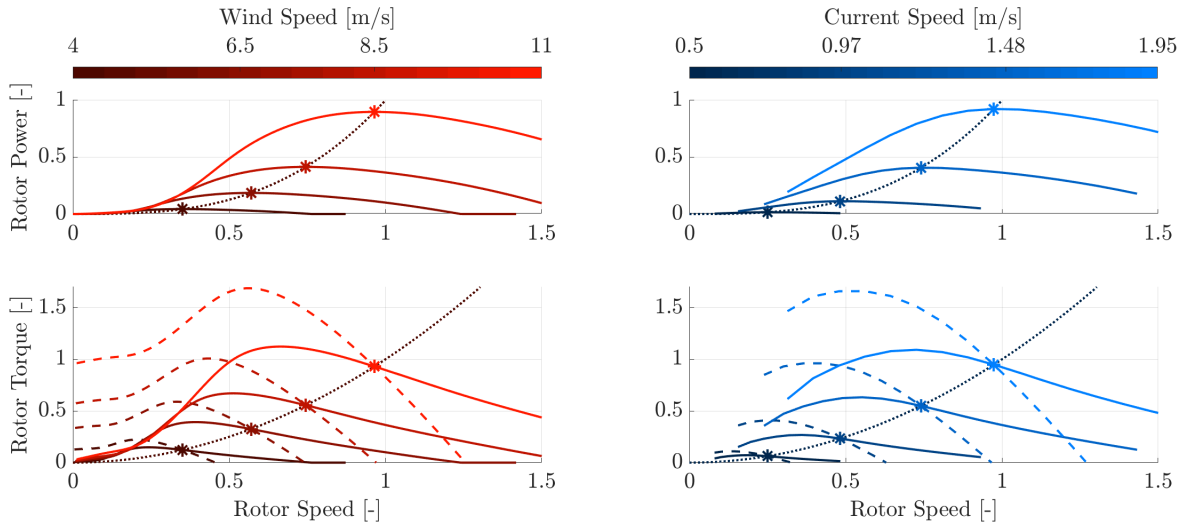

Figure 1. Performance curves for the reference wind (left) and marine (right) turbines shown at a set of Region 2 flow speeds, where each curve represents steady-state performance (normalized to rated) across rotor speeds with a fixed flow speed. The dotted curves in each plot show the steady-state equilibrium points of Eqs. (5) and (6) tracking maximum power. The upper plots show rotor power ($*$ marks the intersection at the maximum of each power curve), and the lower plots show rotor torque (the dashed curves show the influence of baseline control).

2.2. Torque Control

The objective of this Region 2 controller is to regulate the rotor speed so that the power remains near its maximum, either directly by regulating $\Omega \approx \Omega^*$, or indirectly by following an unknown equilibrium. The controllers introduced in this section are shown in a block diagram in Fig. 2.

2.2.1. Baseline Controller The baseline control law is derived by using the steady-state relationship (Eq. (6)) as a nonlinear control law feeding back transient speed variations instead of as a steady-state reference. This is the well-known

$$\tau = K \left(N_{\text{gb}}\Omega\right)^2, \tag{7}$$

often referred to by the literal name of the calculation performed ("$K\Omega^2$") and employed in many controllers in the literature [4, 5, 2]. One major drawback is its inflexibility, only describing a set of power-maximizing equilibrium points in Region 2 and reducing the first-order settling time by a fixed amount (see Figs. 1 and 3). A simple combination of the $K\Omega^2$ controller with a Region 3 blade-pitch controller may also exacerbate disruptive behavior during controller switching near the transition between Region 2 and Region 3 flow speeds. In ROSCO, this is sidestepped by switching to a more flexible reference-tracking torque controller near the transition region, and the usage of the $K\Omega^2$ controller is superseded in many cases by reference-tracking controllers that achieve the same steady-state performance but with greater control over transient response.

2.2.2. Reference-Tracking Controller An alternative to $K\Omega^2$ control is to generate a nonlinear rotor-speed reference Ω_{ref} tracking the optimal TSR and use a linear torque controller to regulate the rotor speed toward this reference. A simple and common approach for reference-tracking control uses proportional-integral (PI) feedback with tunable gains k_p and k_i as follows:

$$\tau = k_p \left(\Omega - \Omega_{\text{ref}}\right) + k_i \int \left(\Omega - \Omega_{\text{ref}}\right) dt. \tag{8}$$

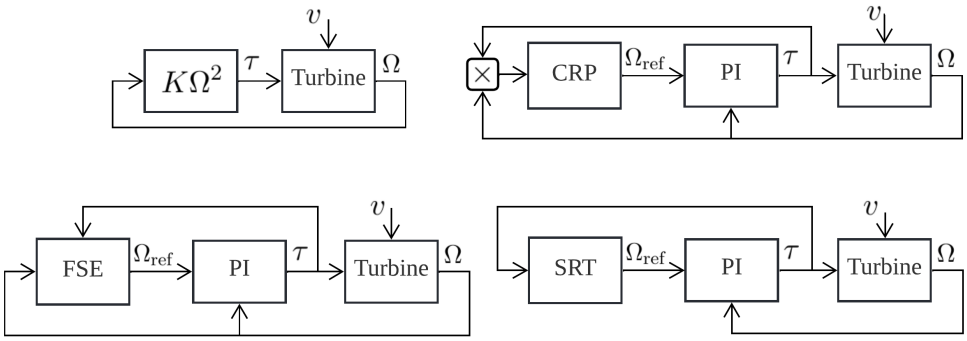

Figure 2. Block diagram representation of the input-output connections for the controllers studied in this paper. Counterclockwise from top left: baseline, flow-speed-estimator reference, square-root-torque reference, cube-root-power reference.

The integral term drifts to follow the reference with zero steady-state error as it ranges from cut-in to rated flow speeds. The transient response of the PI controller is assumed to be on a sufficiently separated time scale from the variation in Ω_{ref}, but the method used to generate Ω_{ref} still may impact closed-loop performance.

2.3. Rotor-Speed Reference Controller

The reference controller generates a speed reference Ω_{ref} attempting to follow the optimal set point Ω^*, which varies in time with a turbulent flow field. This acts as an outer control loop, providing an input to the PI controller functioning as an inner loop. Although the optimal set point is not known exactly, it can be estimated based on measured signals. Depending on the signal source, this estimated optimal set point $\hat{\Omega}^*$ may react to undesired high-frequency contents in the flow turbulence, so it is first filtered to prevent unwanted frequencies from reaching Ω_{ref}. A first-order low-pass filter with a tunable cutoff frequency is used in this work,

$$\dot{\Omega}_{\text{ref}} = \frac{1}{T_f}\left(\hat{\Omega}^* - \Omega_{\text{ref}}\right), \tag{9}$$

where T_f is the time constant of the low-pass filter (inverse of cutoff frequency). The focus of this paper is to analyze and compare different methods of deriving the optimal set point estimate $\hat{\Omega}^*$, which are described in the following subsections. All choices of set point estimate share the property that the closed-loop system is in equilibrium when $\Omega = \Omega_{\text{ref}} = \hat{\Omega}^* = \Omega^*$, but the transient responses may differ, and different nonlinear approaches may lead to different bias in the mean performance. The coupled behavior between the inner (Eq. (8)) and outer (Eq. (9)) loops for each controller will be analyzed in Section 3.

2.3.1. Flow-Speed-Estimator Reference The optimal TSR can be tracked directly by estimating the flow speed based on measured signals of the rotor. A flow-speed estimator (FSE) allows the flow speed v to be used in a feedback loop without measuring it directly but instead deriving the reference based on the estimated flow speed $\hat{v}$. This signal is then used with Eq. (4) to estimate the optimal rotor-speed set point

$$\hat{\Omega}^*_{\text{FSE}} = \frac{\lambda^* \hat{v}}{R}. \tag{10}$$

There are multiple options for dynamic estimator design, with varying levels of performance and complexity. An integral-augmented immersion and invariance filter has been used to estimate the inflow velocity based on PI feedback of rotor speed and a simple tuning structure [6]. The FSE

used in ROSCO is a continuous-discrete extended Kalman filter, described in [2], with more complexity and potential for improved tracking bandwidth. For consistency with the other controllers, the FSE is assumed to have continuous-time dynamics in this analysis, but the implementation with discrete-time update steps is fully described in [2]. The extended Kalman filter estimates low- and high-frequency components of the wind speed $\hat{v}_m$ and $\hat{v}_t$, assumed to be driven by independent process noise inputs of known standard deviation, and the complete estimated flow speed is $\hat{v} = \hat{v}_m + \hat{v}_t$. The nonlinear dynamics (Eq. (3)) are used to propagate the rotor-speed estimate $\hat{\Omega}$, which is then corrected from measurements of true Ω using an optimal linear gain constructed from the linearization of Eq. (3) and an estimate covariance matrix discussed in [2]. In continuous-time, the estimator dynamics are

$$\begin{bmatrix} \dot{\hat{\Omega}} \\ \dot{\hat{v}}_t \\ \dot{\hat{v}}_m \end{bmatrix} = \begin{bmatrix} \frac{1}{J_{\text{rot}}} \left(T_{\text{rot}} \left(\hat{\Omega}, \hat{v} \right) - N_{\text{gb}} \tau \right) \\ -\frac{\pi \hat{v}_m}{12R} \hat{v}_t \\ 0 \end{bmatrix} - \boldsymbol{L}_{\mathbf{FSE}} \left(\hat{\Omega} - \Omega \right), \tag{11}$$

where $\boldsymbol{L}_{\mathbf{FSE}}$ is the time-varying optimal Kalman gain. In the discrete-time implementation [2], the innovation update steps are carried out in a staggered order to take advantage of the best-known estimate of the linearized operating point, but with a fast enough sampling time for the controller, this process is approximated by continuous-time dynamics.

2.3.2. Square-Root-Torque Reference By inverting the monotonic speed-torque relationship (Eq. (6)), we can relate the estimated optimal set point to the square root of generator torque with

$$\hat{\Omega}^*_{\text{SRT}} = \frac{1}{N_{\text{gb}}} \sqrt{\frac{\tau}{K}}, \tag{12}$$

denoted the square-root torque (SRT) set point estimate Ω^*_{SRT}. The SRT reference (Eq. (12)) feeds the control action τ back into the speed reference, using the integral drift of the PI controller to estimate the current set point.

2.3.3. Cube-Root-Power Reference Another approach inverts the monotonic speed-power relationship (Eq. (5)) to relate the estimated optimal set point to generator power with

$$\hat{\Omega}^*_{\text{CRP}} = \frac{1}{N_{\text{gb}}} \sqrt[3]{\frac{P}{K}}, \tag{13}$$

denoted the cube-root power (CRP) set point estimate Ω^*_{CRP}. Feedback of power P includes implicit feedback of both rotor speed and generator torque through Eq. (2).

3. Control Analysis

Analysis of the transient characteristics of the turbine and controllers can be performed using the linearization of each component in the closed-loop system. During operation, the flow speed variation due to turbulence is small and assumed local to a slowly moving average, so the system can be approximated by a linear time-invariant system with fixed parameters for a practically long time span as the controller gradually tracks the set point of the average inflow velocity. The model parameters are taken from two reference axial-flow turbines: the DTU 10 MW wind turbine [7] and the RM1 marine turbine [8]. Some parameter values for these turbines are presented in Table 1.

Table 1. Parameter values for the DTU 10 MW and RM1 reference turbines.

Reference Turbine	**DTU 10 MW** [7]	**RM1** [8]
Fluid density ρ [kg/m^3]	1.225	1,025
Blade length R [m]	89	10
Rotor inertia J_{rot} [kg m]	1.5975×10^8	4.8402×10^5
Gearbox ratio N_{gb} [-]	50	53
Rated flow speed v_{rated} [m/s]	11.4	2.0
Rated power P_{rated} [MW]	10	0.5
Rated rotor speed Ω_{rated} [rad/s]	1.005	1.204
Rated rotor speed Ω_{rated} [RPM]	9.6	11.5
Optimal TSR λ^* [-]	8.0	6.4
Region 2 gain K $\left[\text{kg} \cdot \text{m}^2\right]$	83.32	1.944

3.1. Linearization Analysis

To perform the linearization, we define a perturbation for each signal variable x as $x = \overline{x} + \tilde{x}$, where $\overline{x}$ is the equilibrium value at an operating point and $\tilde{x}$ is the perturbation from the equilibrium. The operating points are constrained to a unique power-maximizing equilibrium with respect to the flow speed $\overline{v}$ as shown in Section 2. After linearization, frequency analysis can be applied to better understand the behavior of the system. A relevant metric for axial-flow turbine performance is the sensitivity of system outputs to the turbulent flow disturbance, so we will examine the frequency response from the input disturbance $\tilde{v}$ to some signals of importance to the controllers.

3.1.1. Linearized Turbine Dynamics At the operating point $\overline{v}$, the rotor dynamics in Eq. (3) are linearized to be

$$J_{\text{rot}}\dot{\tilde{\Omega}} = \frac{\partial T}{\partial \Omega}\tilde{\Omega} + \frac{\partial T}{\partial v}\tilde{v} - N_{\text{gb}}\tilde{\tau}, \tag{14}$$

where $\frac{\partial T}{\partial \times}$ are sensitivity gradients of the rotor inflow torque evaluated at the operating point. Without control input, we can express the system in Eq. (14) as a transfer function from the disturbance $\tilde{v}$ to rotor speed $\tilde{\Omega}$ as

$$\frac{\tilde{\Omega}}{\tilde{v}}(s) = \frac{\frac{\partial T}{\partial v}}{J_{\text{rot}}s - \frac{\partial T}{\partial \Omega}}, \tag{15}$$

with s the Laplace variable. The open-loop turbine dynamics have a single real pole at $s = \frac{1}{J_{\text{rot}}}\frac{\partial T}{\partial \Omega}$. This quantity is inversely related to the first-order time constant of the system, shown for the reference turbines (open-loop and with the baseline controller) in Fig. 3, indicating how quickly each system responds to inputs or settles from a nonzero initial condition. The figure shows that the response of the marine turbine is about an order of magnitude faster than that of the wind turbine, meaning it will more rapidly correct a speed offset from equilibrium.

3.1.2. Baseline Controller The linearization of the baseline controller (Eq. (7)) is

$$\tilde{\tau} = \left(2KN_{\text{gb}}^2\overline{\Omega}\right)\tilde{\Omega}. \tag{16}$$

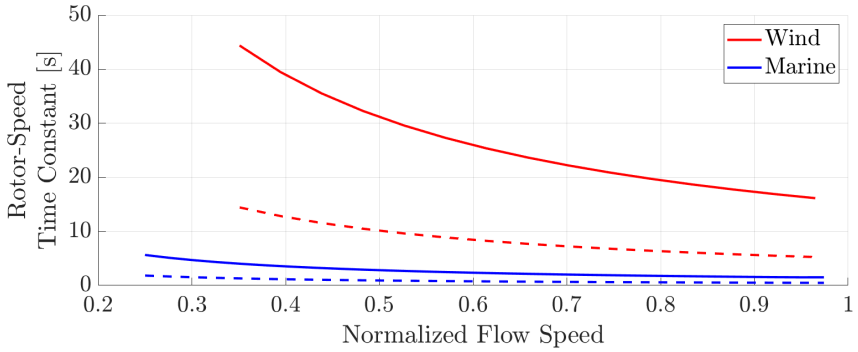

Figure 3. First-order settling time constant, derived from the aerodynamic sensitivities of the linearized turbine model (Eq. (14)), plotted against Region 2 flow speeds normalized to the rated speed. Data are from the DTU 10 MW and RM1 reference turbines. The dashed lines show the same first-order time constant with the influence of the baseline controller, linearized as an effective proportional control loop.

From this form, we see that the baseline $K\Omega^2$ controller is first-order identical to a proportional controller, but the effective proportional gain grows directly with the equilibrium rotor speed $\overline{\Omega}$. With the baseline controller in the loop, the transfer function from flow turbulence to generator speed is

$$\frac{\tilde{\Omega}}{\tilde{v}}(s) = \frac{\frac{\partial T}{\partial v}}{J_{\text{rot}}s - \frac{\partial T}{\partial \Omega} + 2KN_{\text{gb}}^3\overline{\Omega}}, \tag{17}$$

and the pole moves further to the left to $s = \frac{1}{J_{\text{rot}}}\left(\frac{\partial T}{\partial \Omega} - 2KN_{\text{gb}}^3\overline{\Omega}\right)$ with a faster time constant. This time constant is shown by the dashed lines in Fig. 3.

3.1.3. PI Reference-Tracking Controller For all reference-tracking controllers, the inner loop PI controller is a linear system with two inputs, $\tilde{\Omega}$ and $\tilde{\Omega}_{\text{ref}}$, and one output $\tilde{\tau}$, and its linearization is identical to Eq. (8). Using a minimum realization time-domain model, one additional state is required to represent the integral component. In the inner/outer loop reference-tracking controllers (see Fig. 2), the formulation of the controller is completed by coupling the linearized inner loop dynamics with those of the outer-loop reference controller.

The inner-loop control gains are tuned without accounting for the dynamics of the reference using the ROSCO toolbox. The closed-loop system with the PI controller (Eq. (8)) is parameterized as a standard second-order system with a characteristic natural frequency ω_{PI} and damping ratio ζ_{PI}. See [2] for details on autotuning the PI gains using these parameters. For this work, the controllers for both the wind and marine turbines were tuned with a natural frequency $\omega_{\text{PI}} = 0.4$ rad/s and damping ratio $\zeta_{\text{PI}} = 1.0$, and a time constant of $T_f = 20$ s.

3.1.4. FSE Reference While the extended Kalman filter utilizes a more precise time-varying linearization of the model to construct the gain $\boldsymbol{L}_{\mathbf{FSE}}$, this analysis is performed around the static equilibrium states in the power-maximizing operating schedule. The estimator states are at equilibrium with $\overline{\hat{\Omega}} = \overline{\Omega}$, $\overline{\hat{v}}_m = \overline{v}$, and $\overline{\hat{v}}_t = 0$, and the steady-state optimal estimator

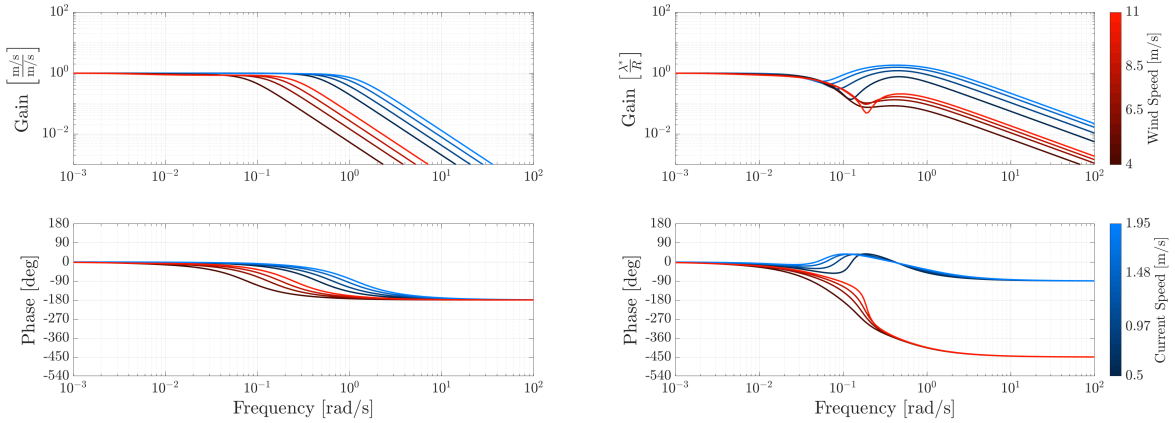

Figure 4. Bode plots of the FSE estimate (left) and for the closed-loop system with the FSE controller (right) for the DTU 10 MW (red) and RM1 (blue) reference turbines.

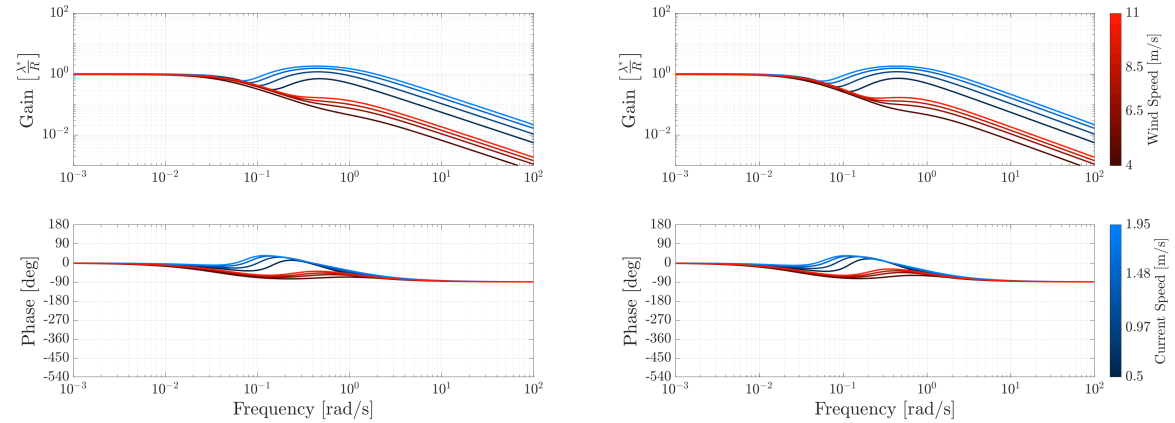

Figure 5. Bode plots of the linearized closed-loop model with the SRT controller (left) and the CRP controller (right) for the DTU 10 MW (red) and RM1 (blue) reference turbines.

gain $\overline{\boldsymbol{L}}_{\mathbf{FSE}}$ is the solution to the algebraic Riccati equation. The linearized estimator model is

$$\begin{bmatrix} \dot{\tilde{\hat{\Omega}}} \\ \dot{\tilde{\hat{v}}}_t \\ \dot{\tilde{\hat{v}}}_m \end{bmatrix} = \begin{bmatrix} \frac{1}{J_{\text{rot}}}\frac{\partial T}{\partial \Omega} & \frac{1}{J_{\text{rot}}}\frac{\partial T}{\partial v} & \frac{1}{J_{\text{rot}}}\frac{\partial T}{\partial v} \\ 0 & -\frac{\pi \overline{v}}{12R} & 0 \\ 0 & 0 & 0 \end{bmatrix} - \overline{\boldsymbol{L}}_{\mathbf{FSE}} \left(\tilde{\hat{\Omega}} - \tilde{\Omega} \right) + \begin{bmatrix} \frac{-N_{\text{gb}}}{J_{\text{rot}}} \\ 0 \\ 0 \end{bmatrix} \tilde{\tau} \tag{18}$$

$$\tilde{\hat{v}} = \tilde{\hat{v}}_t + \tilde{\hat{v}}_m, \quad \tilde{\hat{\Omega}}^*_{\text{FSE}} = \frac{\lambda^* \tilde{\hat{v}}}{R}, \tag{19}$$

and the dynamic optimal set point estimate (Eq. (19)) is filtered with the linear low-pass filter (Eq. (9)) to drive the reference $\tilde{\Omega}_{\text{ref}}$. Combining these dynamics with inner-loop controller (Eq. (8)) and the turbine (Eq. (14)) completes the closed-loop FSE model. The frequency response from the inflow speed $\tilde{v}$ to the estimate (Eq. (19)) is shown on the left side of Fig. 4, and the closed-loop transfer function from $\tilde{v}$ to $\tilde{\Omega}$ is shown on the right.

3.1.5. SRT and CRP Reference For the static (non-FSE) reference-tracking controllers, the optimal set point estimate can be modeled by utilizing the gradients of the function $\hat{\Omega}^*$:

$$\dot{\tilde{\Omega}}_{\text{ref}} = \frac{1}{T_f}\left(\frac{\partial\hat{\Omega}^*}{\partial\Omega}\tilde{\Omega} + \frac{\partial\hat{\Omega}^*}{\partial\tau}\tilde{\tau} - \tilde{\Omega}_{\text{ref}}\right), \tag{20}$$

where the total derivative of the set point estimate function $\hat{\Omega}^*$ is expanded in perturbations of the arguments $\tilde{\Omega}$ and $\tilde{\tau}$. For each of these partial derivatives, a nonzero value indicates implicit feedback of the respective signal. For the SRT controller, the gradients are

$$\frac{\partial\hat{\Omega}^*}{\partial\Omega} = 0;\ \frac{\partial\hat{\Omega}^*}{\partial\tau} = \frac{1}{2KN_{\text{gb}}^2\overline{\Omega}}, \tag{21}$$

with zero direct feedback of $\tilde{\Omega}$. For the CRP controller, the gradients are

$$\frac{\partial\hat{\Omega}^*}{\partial\Omega} = \frac{1}{3};\ \frac{\partial\hat{\Omega}^*}{\partial\tau} = \frac{1}{3KN_{\text{gb}}^2\overline{\Omega}}, \tag{22}$$

with implicit feedback of both speed and torque. The closed-loop models for SRT and CRP are similarly constructed by combining Eq. (20) (using the above coefficients) with the inner-loop controller, Eq. (8), and turbine model, Eq. (14). Bode plots of the SRT and CRP controllers are shown in Fig. 5. The frequency responses of each model are nearly identical, a consequence of sharing tuning values for T_f, k_p, and k_i and the linearized form (Eq. (20)), despite different values of the derivatives of $\hat{\Omega}^*$ populating Eq. (20).

4. Simulation Results

The baseline, FSE, SRT, and CRP controllers were simulated in OpenFAST with the Technical University of Denmark (DTU) 10 MW and Reference Model 1 (RM1) turbine models. At each Region 2 flow speed, there were six random turbulence seeds of 10 minutes each after initial conditions had settled. The wind turbulence had a 16% turbulence intensity, while the water current turbulence had a constant standard deviation of 0.25 m/s (amounting to a turbulence intensity of 100% at cut-in and 25% at rated). The rotor speed and generator power statistics are shown in Fig. 6.

For the wind turbine, every reference-tracking controller showed a decrease in rotor-speed variation by about 10–20%, while the power variation decreased at low wind speeds and increased near rated. The mean power decreased by less than 1% for all controllers at low wind speeds, and the CRP controller also caused about 2% decrease in mean rotor speed compensated by an increase in mean torque (not shown).

For the marine turbine, performance differences varied more substantially across current speeds, with the FSE controller increasing speed and power variation more at higher flow speeds. The reference-tracking controllers all suffered some mean power losses at lower flow speeds, possibly a consequence of the increased power variation. While the SRT and baseline controllers had nearly the same mean rotor speed, the CRP and FSE controllers found a different mean rotor speed to be mostly consistent across flow speeds. This translates to a difference in mean TSR by a few percent between the controllers.

5. Conclusions and Future Work

Several reference-tracking torque controllers have been surveyed and compared to a standard $K\Omega^2$ baseline for application in a wind and marine turbine. The control design approach was

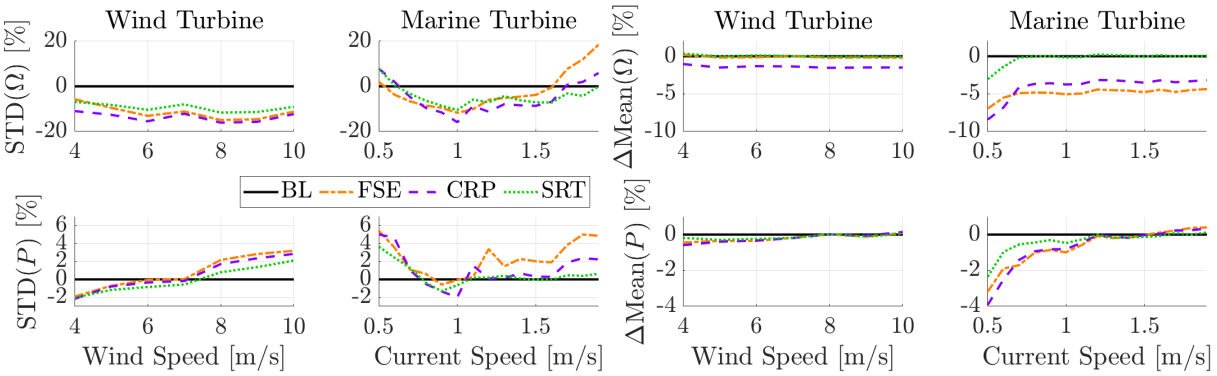

Figure 6. OpenFAST simulation statistics for the DTU 10 MW and RM1 reference turbines simulated under turbulent inflow with mean velocities from cut-in to just below rated (see Table 1). The standard deviation and mean of rotor speed Ω and generator power P are shown as normalized percent difference to baseline across 10-minute-average flow speeds.

geared toward a wind turbine, but the analytical similarity between the wind and marine turbine models justifies a unified process for control analysis in both applications. Each controller improved performance for the wind turbine as expected, but the FSE controller struggled in the marine case at high current speeds. This may be improved by replacing the FSE in the marine application, but for the purpose of unified design, the SRT and CRP controllers show some improvement for the marine case as well. In the simulation results of the tested controllers, the reference-tracking controllers group together distinctly from the baseline, while differing trends between the wind and marine turbines suggest that there is more work to be done optimizing the design of wind energy controllers for the marine energy application to achieve comparable performance improvement.

Optimizing the tuning of each controller for each turbine should be investigated further. With comparable simulation performance, reasons to prefer one controller over another may be due to other design aspects not factored into this analysis. The transition into Region 3 for a pitch-actuated turbine may include modifying the reference of the torque and pitch controllers to smooth out the transition [2], for which any of the reference controllers is more suitable than the baseline. Fixed-pitch control in Region 3 follows operating points defined using different functions (such as inverse torque), so the most appropriate controller for such an application may depend more strongly on the ease of transition into the Region 3 reference function than any subtle difference in Region 2 performance. For the purpose of supervisory control, estimating flow speed serves additional utility beyond providing a reference to the torque controller.

Acknowledgments
This work was authored in part by the National Renewable Energy Laboratory, operated by Alliance for Sustainable Energy, LLC, for the U.S. Department of Energy (DOE). This work was funded in part by the U.S. Department of Energy Office of Energy Efficiency and Renewable Energy Wind Energy Technologies Office, and by a Palmer Endowed Chair at the University of Colorado Boulder. The views expressed in the article do not necessarily represent the views of the DOE or the U.S. Government. The U.S. Government retains and the publisher, by accepting the article for publication, acknowledges that the U.S. Government retains a nonexclusive, paid-up, irrevocable, worldwide license to publish or reproduce the published form of this work, or allow others to do so, for U.S. Government purposes.

References

[1] Kilcher L, Fogarty M and Lawson M 2021 Tech. Rep. NREL/TP-5700-78773 NREL Golden, CO
[2] Abbas N, Zalkind D, Pao L Y and Wright A 2022 *Wind Energy Science*
[3] NREL 2023 OpenFAST URL `https://github.com/OpenFAST/openfast`
[4] Johnson K E, Pao L Y, Balas M J and Fingersh L J 2006 *IEEE Ctrl. Sys. Mag.*
[5] Pao L Y and Johnson K E 2011 *IEEE Ctrl. Sys. Mag.*
[6] Brandetti L, Mulders S P, Liu Y, Watson S and van Wingerden J W 2023 *Wind Energy Science Disc.*
[7] Bak C, Zahle F, Bitsche R *et al.* 2013 Tech. Rep. I-0092 DTU Wind Energy
[8] Neary V S, Lawson M, Previsic M *et al.* 2014 *Proc. Marine Energy Tech. Symp.*